Progress in Sky Radiance and Luminance Modeling Using Circumsolar Radiation and Sky View Factors

Christian A. Gueymard[1] and Stoyanka Ivanova[2]

[1] Solar Consulting Services, Colebrook, NH (USA)

[2] University of Architecture, Civil Engineering and Geodesy, Sofia (Bulgaria)

Abstract

The main applications of radiance/luminance models are reviewed here, with an emphasis on empirical models based on experimental data, typically provided by sky scanners. Such measurements, and the derived models, are subject to various limitations. Nevertheless, the Igawa radiance model is validated under the high-elevation and low-turbidity conditions of Colorado, and found reasonably accurate under both clear and cloudy conditions. Here, the Igawa model is enhanced by combining it with a new parameterization of the clear-sky circumsolar radiance to improve the overall radiance prediction within the aureole region. This results in the turbidity-dependent IGI model. Based on this new anisotropic radiance model, a real sky view factor (RSVF) for partially obstructed skies can be used as a basis for realistic calculations. It can be calculated with the SOLARES software, which is designed to accept irradiance inputs from, e.g., a typical meteorological year (TMY), and thus can be used to provide hourly results at any location where a TMY or an irradiance time series is available. A simulation is performed for an ideal solar system with or without sky obstruction and compared to the classic SVF approach, resulting in significant differences. The proposed approach can be advantageously used in lieu of the conventional isotropic SVF method in many types of shading geometry in the built environment.

Keywords: Sky radiance; Luminance; Shading; Radiative transfer; Aerosols; Circumsolar radiation; Sky view factor

1. Introduction

The main goal of a radiance model is to describe the radiant energy emitted from any point of the sky. Luminance is similar to radiance, but after adaptation to the spectral range of human vision. A radiance/luminance model has two purposes: (i) to assist the understanding of the directional properties of solar irradiance or illuminance at the earth surface, and their bearing on various atmospheric constituents, most importantly aerosols and clouds; and (ii) to serve various applications in many fields, such as engineering, architecture, forestry, photobiology or climatology. The literature on these topics is quite abundant. In particular, the determination of the sky diffuse radiance under cloudless conditions has been at the center of many developments in atmospheric scattering theory and radiative transfer for decades. Bullrich (1964) offered one early review of such developments. More recently, it is worthwhile to underline the theoretical work that allows a precise determination of the sky radiance distribution from the aerosol optical properties (Burley et al., 2017; Kocifaj, 2009, 2012, 2015; Liang and Lewis, 1996; Zibordi and Voss, 1989). Conversely, the measurement of sky radiance is at the core of *inversion* methods that aim at deriving some essential aerosol properties (Dubovik and King, 2000; Nakajima et al., 1996; Oliveros et al., 1998; Qin et al., 2002).

All the models just mentioned are of a *spectral* nature, which entails a high level of complexity (including the need for specialized inputs) that makes them typically incompatible with most applications in solar engineering or architecture, for instance. For such applications, many simpler models of a *broadband* nature have been developed over the years. Both radiance and luminance models of this type can be classified into either clear-sky models (e.g., Gueymard, 1986; Harrison and Coombes, 1988; Vida et al., 1999) or all-sky models (e.g., Brunger and Hooper, 1993; Igawa, 2014; Kocifaj, 2011; Kocifaj and Gueymard, 2017; Perez et al., 1993; Rosen et al., 1989). A partial review of such models was proposed by Torres and Torres (2008).

doi:10.18086/eurosun2018.09.16 Available at http://proceedings.ises.org

Like irradiance, radiance has two different components—direct (beam) and diffuse. For simplification, the direct component is usually considered as emanating from a simple point source at the center of the sun disk. The diffuse radiance distribution over the whole sky hemisphere is not trivial and has been the topic of many experimental or theoretical investigations, as reviewed above. From a solar engineering standpoint, the integrated diffuse radiance from the visible sky parts leads to the estimation of the diffuse irradiance under a partly obstructed sky. Related tasks are the determination of the diffuse irradiance on tilted planes or of the optimal tilt and azimuth of solar systems (Li and Lam, 2007; Smith et al., 2016), particularly in the presence of obstructions (Lou et al., 2016). A convenient way to solve diffuse shading calculations is to rely on the *sky view factor* (SVF) concept. Whereas, in general, this assumes that the sky radiance is isotropic, it is now possible to take into account the actual anisotropy of the radiance/luminance (Ivanova and Gueymard, 2018). In parallel, sky luminance models are important for architectural and daylighting applications since they condition the illuminance (or daylight availability) inside buildings (Acosta et al., 2015; Darula et al., 2015).

In the engineering or architectural practice, all radiance/luminance models in current use are based on an empirical representation of experimental data, typically provided by sky scanners (Brunger and Hooper, 1991; Harrison and Coombes, 1988; Igawa, 2014; Wittkopf and Soon, 2007). Such measurements—and the derived models—are subject to various limitations, particularly in the circumsolar region (or "aureole"). That region is particularly bright when the sun and its immediate proximity are either unobscured (clear sky) or obscured with a thin layer of cirrus cloud (Blanc et al., 2014). The present investigation is aimed at exploring improvement possibilities on these limitations, and at developing a radiance/luminance model amenable to the precise calculation of anisotropic sky view factors.

2. Experimental and modeling limitations

Most sky scanners implement the Tregenza (1987) method of mapping the sky into elements, or "patches", of roughly equal angular size (≈0.2 rad). Although Tregenza's original design called for 151 such patches, in later experimental implementation this number was reduced to 145, for reasons explained elsewhere (Subramaniam and Mistrick, 2017). This low number of elements entails a coarse spatial resolution. Moreover, a complete sky scan takes a few minutes to complete, which indicates a coarse temporal resolution as well, and a likely risk of errors under rapidly changing sky conditions. Furthermore, due to stray-light contamination, no accurate measurement can be made within 15–20° from sun center. This limitation means that the bright aureole surrounding the sun cannot be modeled correctly from such data. Similarly, the radiance near the horizon cannot be measured precisely due to contamination from surface reflections. Hence, the radiance/luminance model developed by Igawa (2014), for instance, is based on measured datasets that exclude all radiance observations that are within 18° of sun center or within 6° of the horizon. Consequently, the radiance/luminance models empirically derived from such data cannot predict the circumsolar radiance reliably, and tend to underestimate it since it is much brighter there than elsewhere under clear conditions, in particular. A method to alleviate this issue is investigated in what follows.

Aerosol particles scatter intensely in the forward direction, which explains the brightness of the sun aureole region. The angular intensity of this scattering is described by a *phase function* that is specific to each type of aerosol, and thus varies over time and space. (Alternatively, this quantity is referred to as "indicatrix" in the luminance literature (Kittler, 1994).) For simplification, the empirical radiance/luminance models of the literature do not use any specific information on aerosol type, or even turbidity, which prevents a correct modeling of the radiance in the aureole. This is exemplified in Fig. 1, which compares the clear-sky diffuse radiance in the principal plane (i.e., the vertical plane containing the sun and the zenith), as predicted by four models of the literature that are representative of two distinct groups: Turbidity-independent models (Brunger and Hooper, 1993; Igawa, 2014) vs. turbidity-dependent models (Gueymard, 1986; Vida et al., 1999). The radiance is normalized by the diffuse horizontal irradiance, evaluated here for winter conditions (sun elevation, $h = 30°$ or zenith angle, $Z = 60°$) in Sofia, Bulgaria under clean conditions (characterized by an aerosol optical depth at 1 μm, β, of 0.025). The turbidity-independent models by Brunger and Hooper (1993) and Igawa (2014) agree relatively well, whereas the turbidity-dependent models of Vida et al. (1999) and Gueymard (1986) predict widely different circumsolar radiance. Similar comparisons, involving another set of four models, have been described by Gracia et al. (2011). A method to correctly evaluate the circumsolar radiance components is discussed in Section 4, and an application for the built environment is proposed in Section 5.

Despite its expected lack of accuracy in the solar aureole or close to the horizon, the Igawa (2014) model appears an interesting option for general modeling of *both* radiance and luminance—considering that basically all other models are rather exclusive, i.e., designed to represent *either* radiance *or* luminance distributions. Moreover, Igawa's model is based on a long series of carefully conducted radiance and luminance measurements, and also benefits from a variety of ancillary meteorological observations. All this is conducive to prediction results of potentially good accuracy, at least over areas of similar climate to the urban environments where the measurements were conducted (in Osaka and Tokyo, Japan). To receive general acceptance, the model still needs to be validated in a broader sense. To that effect, a limited validation is conducted at a site with a widely different climate, as discussed in the next Section.

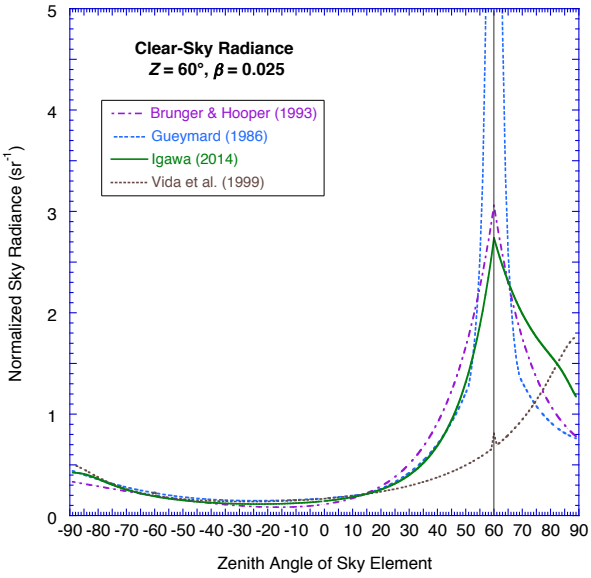

Fig. 1. Sky radiance (normalized by the diffuse horizontal irradiance) in the principal plane obtained by four different models under typical (low-turbidity) conditions for winter in Sofia. The vertical line indicates the sun's position (zenith angle: 60°).

3. Igawa's model performance in Colorado

The National Renewable Energy Laboratory (NREL) conducted three years of measurements (from June 14, 2000 to October 28, 2002) of sky radiance and luminance distribution at 145 sky points with an EKO MS-300LR Sky Scanner. Scans (lasting 3.5 minutes each) were acquired every 15 minutes during the whole day at the Solar Radiation Research Laboratory (SRRL; https://midcdmz.nrel.gov/srrl_bms/) in Golden, Colorado (lat. 39.742°, long. –105.18°, elev. 1828.8 m AMSL). Additionally, the same website offers detailed 1-min global and diffuse solar irradiance data, among many other radiometric or meteorological observations. These two irradiance quantities are the normal input data for Igawa's all-sky luminance and radiance model. Owing to its high elevation, that station experiences a much cleaner atmosphere (lower turbidity) than most urban areas, such as those where Igawa's model was developed.

A preliminary analysis of the measured radiance is required for quality-control purposes. It is found that the scanner reported anomalous null values of radiance much too frequently, signaling either very low radiance values (under the instrument's detection threshold) or possible malfunction in hardware of software. Another problem is that the scanner was apparently not correctly calibrated, as revealed when comparing the horizontally integrated sky radiance with the measured diffuse horizontal irradiance. The ratio between the measured irradiance and the spatially integrated radiance is found equal to 1.53. This correction factor is thus applied as a pseudo calibration coefficient for the validation exercise described below.

Figure 2 illustrates the horizontal projections of sky diffuse radiance, as measured with NREL's sky scanner (left column) and modeled with Igawa's model (right column) during two moments (one per row) of a single cloudy day (2000-06-15). The occasional sky patches with reported null values are displayed in magenta. Visual inspection of a large number of such images proves how precise the Igawa's model reflects the anisotropic nature of sky diffuse radiance.

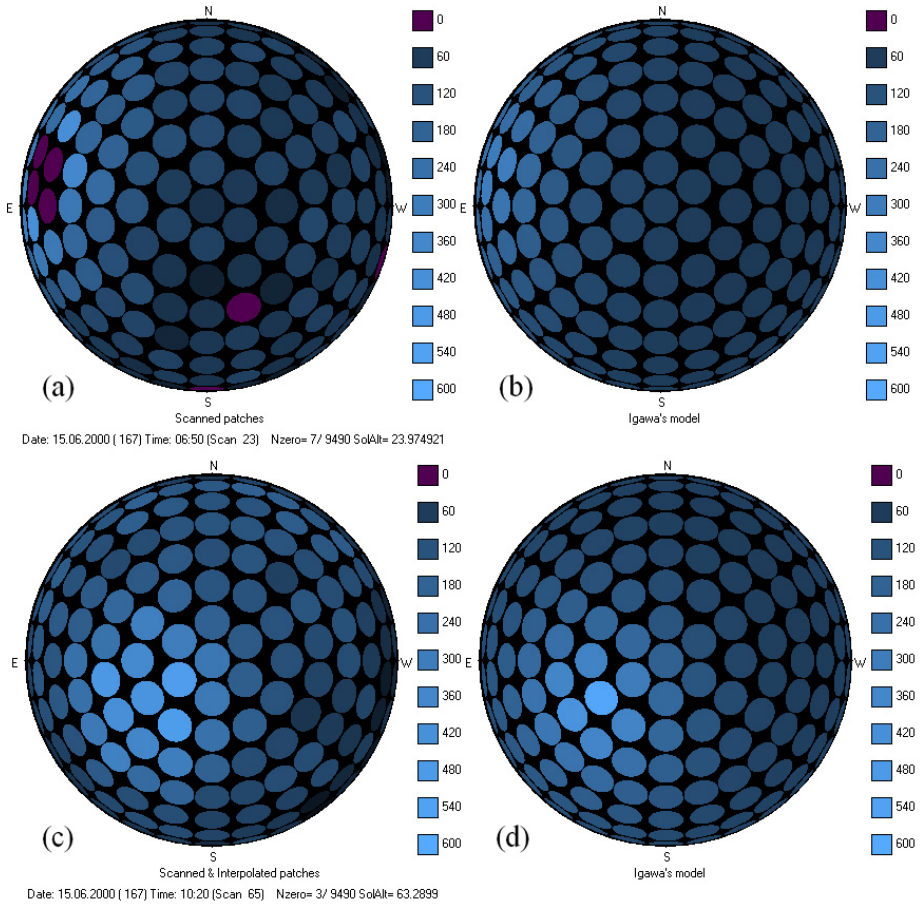

Fig. 2. Horizontal projections of sky diffuse radiance for 145 patches during two moments of a cloudy day, 2000-06-15: (a) Scanned radiance at 06:50 local standard time (magenta circles are for anomalous zero radiance in seven patches); (b) Igawa-modeled radiance at 06:50 for the same 145 patches; (c) Scanned radiance at 10:20 (the radiance in three anomalous null patches is interpolated from their neighbors); (d) Igawa-modeled radiance at 10:20 for the same 145 patches. The solar altitude (SolAlt or *h*) is indicated in each case.

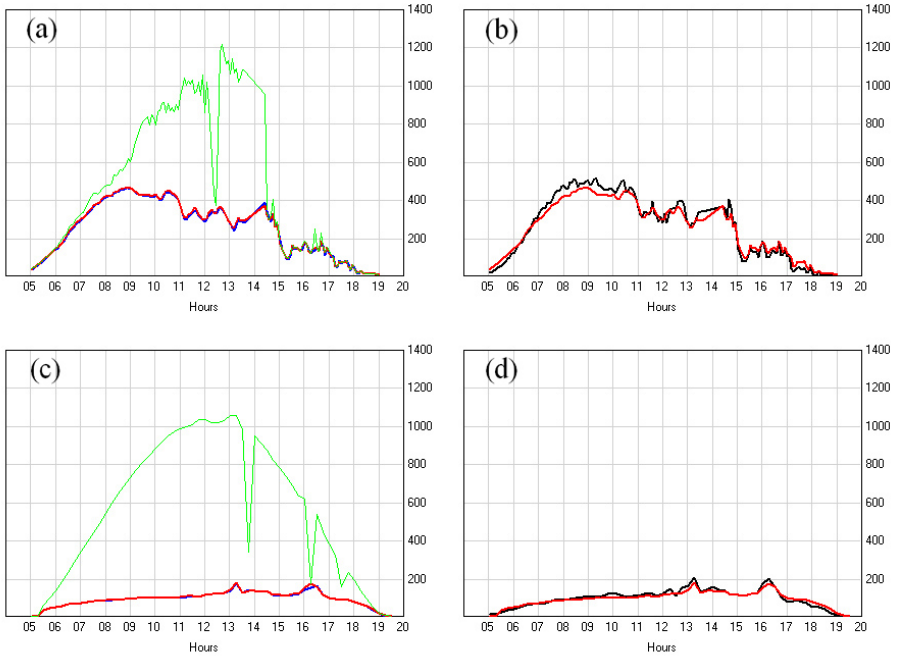

Fig. 3. Components of irradiance measured or modeled at NREL's station in Colorado. Green line is for measured global horizontal irradiance, red line is for measured diffuse horizontal irradiance, blue line is for predicted irradiance using modeled radiance (Igawa, 2014), and black line is for integrated diffuse irradiance from experimental radiance measurements after interpolation of anomalous null patches. (a, b) predominantly cloudy sky, 2000-06-15; (c, d) clear sky, 2000-07-22.

For the same cloudy test day as in Fig. 2, the top row of Fig. 3 indicates the close agreement between the diffuse horizontal irradiance measured with a pyranometer (in red), the predicted diffuse irradiance derived from Igawa's model (in blue), and the spatially integrated measured radiance based on the interpolated scanned values (in black). Similarly, the bottom row of Fig. 3 is for a mostly clear day (2000-07-22). The red and blue lines almost coincide in both cases, which indicates a good performance of the model under varied sky clearness conditions. For the cloudy day, however, the black line of integrated experimental diffuse radiance exceeds the measured diffuse irradiance. This can be caused in part by inadequacies caused by the rapidly changing sky conditions, or by shortcomings in the model under some specific types of clouds.

A more systematic comparison is performed between the diffuse irradiance measured with a pyranometer and that obtained by spatially integrating Igawa's radiance, under favorable conditions ($h > 10°$ and scans with less than 30 null patches). All null patches with zero radiance are substituted with interpolated values, calculated from the radiance of neighboring patches with valid and non-null data. Sky patches considered valid here are those whose center's altitude is more than 6° and that are at a minimum distance of 18° from sun center. Using the estimated values of the modeled diffuse radiance and their deviations in comparison with the scanned values, statistical indicators such as MBD (Mean Bias Deviation), rMBD (relative Mean Bias Deviation, in percent), MAB (Mean of Absolute Bias), and RMSD (Root Mean Square Deviation), are calculated. The results for June and July 2000 are given in Table 1. The daily level of cloudiness is indicated by the diffuse ratio, K, defined as H_d/H, the ratio of the daily diffuse and global horizontal irradiations. K varied between 0.16 and 0.93 during the two months, thus allowing the validation of Igawa's model for very clear to very cloudy sky conditions. Overall, the model is found to behave adequately at the SRRL station, despite its widely different climate than the low-elevation urban climates pertaining to Igawa's model. Due to the experimental limitations encountered here, more validation is desirable at sites using high-resolution sky cameras and emerging processing techniques (e.g., Chauvin et al., 2015), for instance.

Tab. 1: Results from the analysis of radiance and irradiance data for June and July 2000 in Colorado.

Date	Number of scan cycles	K	MBD (W/m^2 sr)	rMBD (%)	MAB (W/m^2 sr)	RMSD (W/m^2 sr)	Modeled/Observed H_d	# Analyzed patches
2000-06-14	110	0.232	-8.4	-11.1	32.4	42.2	0.991	5167
2000-06-15	160	0.522	-11.9	-12.3	34.6	45.9	0.979	13072
2000-06-17	169	0.565	-4.9	-5.0	42.0	55.5	1.079	9924
2000-06-18	169	0.474	-13.0	-13.6	42.5	55.8	0.950	11218
2000-06-19	81	0.518	-2.4	-2.8	44.1	57.0	1.064	2587
2000-06-22	59	0.280	-6.1	-7.5	37.8	48.7	1.097	1725
2000-06-23	59	0.575	-3.5	-3.8	42.7	55.9	1.030	4094
2000-06-24	59	0.440	-5.5	-6.2	50.4	63.6	1.032	3341
2000-06-25	59	0.697	-7.0	-7.3	45.6	58.9	1.057	2584
2000-06-26	59	0.927	-6.3	-10.3	21.0	26.6	1.067	1724
2000-06-28	50	0.707	-5.6	-6.7	30.5	40.1	1.056	2051
2000-07-01	59	0.570	-7.4	-7.6	50.6	64.1	1.059	2800
2000-07-05	59	0.198	-1.4	-2.6	28.7	42.2	1.104	1724
2000-07-10	59	0.289	-7.6	-11.5	40.4	56.4	0.959	3136
2000-07-13	59	0.334	-9.0	-9.5	49.4	64.5	0.998	2047
2000-07-14	59	0.236	-6.2	-8.3	34.7	46.6	1.043	2054
2000-07-16	59	0.725	-15.6	-12.1	48.6	63.2	1.025	2802
2000-07-17	59	0.467	-8.3	-10.4	38.7	51.3	1.012	2700
2000-07-18	59	0.202	2.6	3.9	37.8	47.3	1.098	754
2000-07-20	59	0.189	-9.9	-16.0	36.0	50.4	1.005	1942
2000-07-21	59	0.184	-7.0	-13.6	30.3	44.1	0.996	2372
2000-07-22	59	0.161	-0.9	-2.6	19.3	29.6	1.018	1509

4. Circumsolar radiance

Based on the discussion in Section 2, it is argued here that Igawa's model (as well as essentially all empirical radiance models based on similar sky scanner measurements) cannot be accurate in the circumsolar (CS) region. That region extends from the edge of the sun's disk to a few degrees around it. Although there is no accepted definition of its precise extent, it is important to note that the innermost area within 2.5° of sun center is considered as direct irradiance in field radiometry (Blanc et al., 2014). For the present purpose, the CS area is defined as the sky annulus between the edge of the sun's disk (at ≈0.26° from its center) up to ≈6°.

Thick clouds do not transmit direct irradiance and do not generate CS radiance either. In contrast, thin clouds (like cirrus) do transmit direct irradiance and actually generate high levels of CS radiance (Blanc et al., 2014).

Because of the complexity of modeling such situations, they are not considered in what follows. Rather, a pure clear-sky CS circumsolar radiance model is developed using parameterized results from SMARTS v2.9.8 (Gueymard, 2001). A rural aerosol model is assumed, along with a wide range of zenith angles (0–85°) and of turbidity (β from 0 to 0.6). Denoting ξ (in degrees) as the scattering angle (i.e., the angular distance between sun center and a sky element), the simulated broadband CS radiance can be accurately modeled as

$$L_{CS}/E_d = (A_0 + A_1\xi)/(1 + A_2\xi) \quad \text{(eq. 1)}$$

where E_d is the clear-sky diffuse horizontal irradiance, and A_i (i = 0–2) are intricate functions of both β and relative air mass, m (a pure function of Z); see Appendix. Figure 4 shows two examples of the normalized radiance thus obtained for high-sun (h = 60° or Z = 30°) and low-sun (h = 30° or Z = 60°) conditions and variable turbidity. Note the strong effect of turbidity, and that the maximum normalized radiance is reached for $\beta \approx 0.15$. It is verified that Eq. (1) can be extrapolated to at least ξ = 10°. Because this CS radiance decreases steeply with ξ, it becomes lower than Igawa's clear-sky radiance within typically 2–6° from sun center. Assuming cloudless conditions in the CS area, the CS-corrected radiance model takes the form

$$L_c = \mathrm{Max}(L_{CS}, L_{Ic}) \quad \text{(eq. 2)}$$

where L_{Ic} is Igawa's clear-sky radiance model mentioned above. Examples of results obtained with Eq. (2) are shown in Fig. 5, which is similar to Fig. 1. For the same zenith angle of 60°, the impact of β is obvious. It appears, however, that Eq. (2) translates into a radiance distribution that lacks the expected smoothness at the seams, due to the simplicity of this preliminary version of the overall radiance model described by Eq. (2).

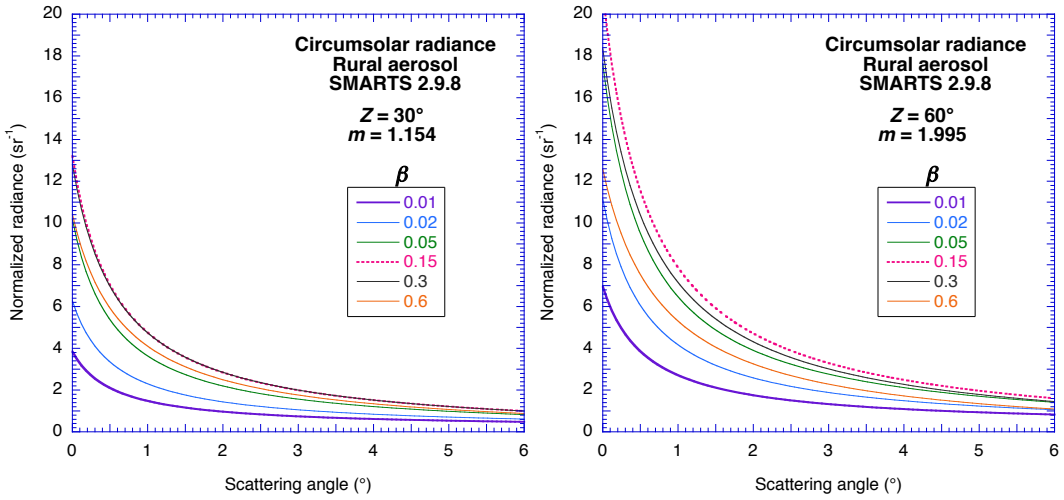

Fig. 4. SMARTS-derived circumsolar radiance for two zenith angles and various turbidity conditions

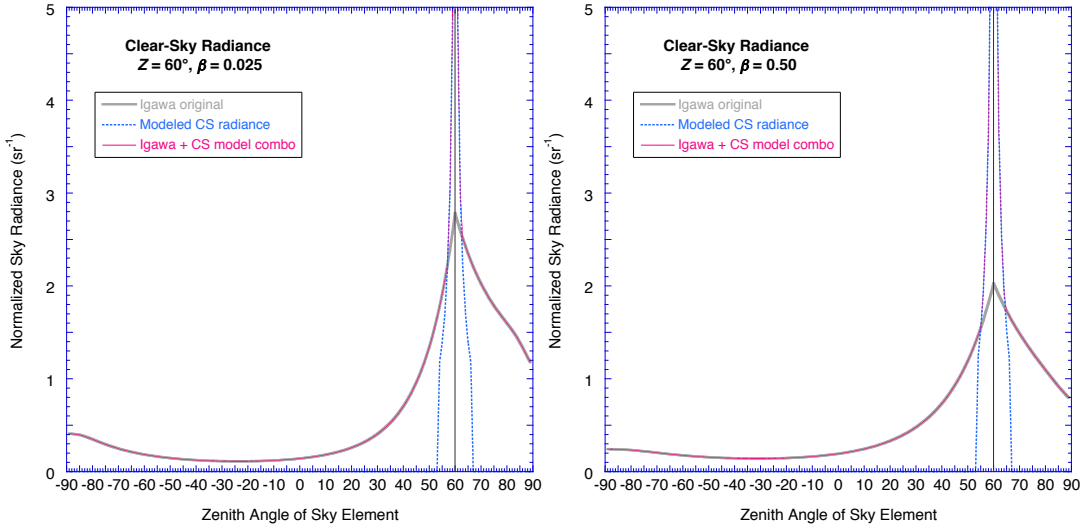

Fig. 5. Clear-sky radiance along the principal plane for very clean conditions (left) and hazy conditions (right), showing the components of Eq. (2)

5. Sky radiance anisotropy and sky view factors

The concept of "Sky View Factor" (SVF) is widely used in many applications. It denotes the ratio between the radiation received by a planar surface and that from the entire radiating (i.e., unshaded) sky hemisphere. For simplification, the "classic" approach is to calculate SVF as the fraction of sky visible from the ground. This implies a simple isotropic diffuse approximation, which states that the radiance (or luminance) is uniform over the whole sky hemisphere. In the general case (e.g., Figs. 1 or 5) this assumption is not realistic, and thus leads to significant errors. In what follows, an example of *anisotropic* SVF for partially obstructed skies, generated with the help of the improved version of an orthographic urban radiance model (Ivanova, 2015), illustrates the gain of accuracy that can be expected in practice by following a more physical method than that based on the conventional isotropic assumption.

For this demonstration, a complete annual set of daily cumulative radiance patterns is prepared with the high-resolution SOLARES model (Ivanova and Gueymard, 2018) for the particular location of Sofia during a single year, 2014. The input dataset consists of the hourly SARAH satellite-derived irradiance values obtained from PVGIS (http://re.jrc.ec.europa.eu/pvg_tools/en/tools.html). In the control experiment, the sky diffuse radiance and tilted irradiance values are calculated with the naïve assumption of an isotropic radiance. This is compared to two slightly different anisotropic approaches: (i) the Igawa model, as published (Igawa, 2014); and (ii) a more involved model obtained by combining that model with the simple circumsolar model described in Section 4, for solar altitudes more than 5° and for sky patches within 6° of sun center. The input data are values of β and clear-sky determinations for the three irradiance components, obtained with hourly atmospheric data from NASA's MERRA-2 reanalysis and the REST2 model (Gueymard, 2008a). In particular, the clear-sky determination of the direct normal irradiance, DNI, is denoted DNI_{clr}. Using these values, the clear-sky diffuse radiance is estimated with Igawa's specific model for clear-sky conditions, L_{Ic}. That radiance is compared with the diffuse radiance estimated with the CS model, again for clear conditions in the aureole. For each hour, the effective whole-sky radiance is obtained as a weighted average of the clear-sky radiance including circumsolar effects and all-sky Igawa radiance:

$$L = FL_c + (1 - F)L_I \qquad \text{(eq. 3)}$$

where F is the direct clear-sky index (i.e., DNI/DNI_{clr}), L_c is the clear-sky radiance from Eq. (2), and L_I is the all-sky Igawa radiance. F is a proxy for the fractional time during which the aureole can be assumed cloudless. The resulting radiance is compared again with Igawa's all-sky radiance and the larger of the two values is stored as the effective diffuse radiance of the corresponding patch, without any temporal interpolation (although this is technically possible). This development uses the same beam radiance as with the pure Igawa model or the control experiment. The new sky radiance model is referred to here as IGI (Igawa-Gueymard-Ivanova).

The usefulness of anisotropic SVF modeling is demonstrated below with two simple examples, one involving an unobstructed sky and the other involving obstructions and partial shading. In both examples, two very long photovoltaic (PV) panel rows are to be located in Sofia, facing south. The optimum angle to maximize its annual sky irradiation is to be determined using the radiance models described above. For this purpose, the global tilted irradiation is estimated for tilts from 0° to 90° using a constant step of 1°. The calculation procedure includes the estimation of the annual diffuse (H_d) and beam (H_b) irradiations on the tilted surface, as well as their sum, H_t. The reflected irradiance is assumed low and is simply ignored.

One appropriate tool to undertake the numerous calculation steps that are necessary to handle the examples above is the SOLARES software (Ivanova and Gueymard, 2018). Typical inputs are time series of the usual hourly irradiation components that can be found in, e.g., Typical Meteorological Year (TMY) files. A preprocessor creates an annual database with daily cumulative beam and diffuse sky radiance patterns, taking into account anisotropic effects into consideration. This information is stored using a sky division scheme with a selectable number of sky patches. In the results discussed below, a high-resolution scheme with 147,457 patches, referred to as "Reinhart MF:32", is used (Fig. 6b). It is considerably more detailed than the conventional 145-patch Tregenza's scheme (Fig. 6a), and thus allows better modeling of the sky radiance. The cumulative database is then used to calculate the direct and diffuse irradiations incident on any tilted plane, with or without shading, with the help of fisheye orthographic projections of the sky hemisphere and shading objects (Ivanova, 2015).

The SOLARES software also provides visualization of the results. For instance, Fig. 7 shows inclined projections of annual sky radiance patterns onto rows of PV panels with different tilts. The sky and the ground (in green) are partially shaded by the closest row of panels. The sky's black shade looks fuzzy because it is averaged over 20 segments, which are positioned at regular intervals along the central panel's height (1 m assumed), and have a different viewpoint to the shading surface. The cumulative beam and diffuse radiances are displayed with different color scales for clarity.

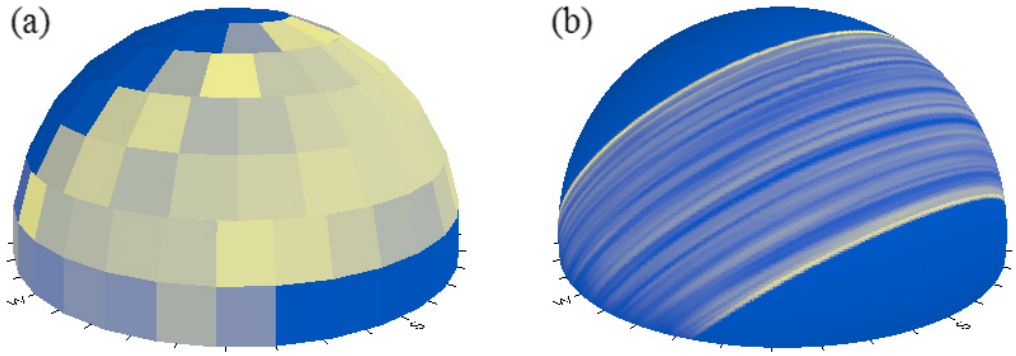

Fig. 6 Continuous sky model of cumulative annual sky radiance pattern, illustrated with different sky division schemes: (a) Tregenza (145 patches); (b) Reinhart-MF:32 (147,457 patches).

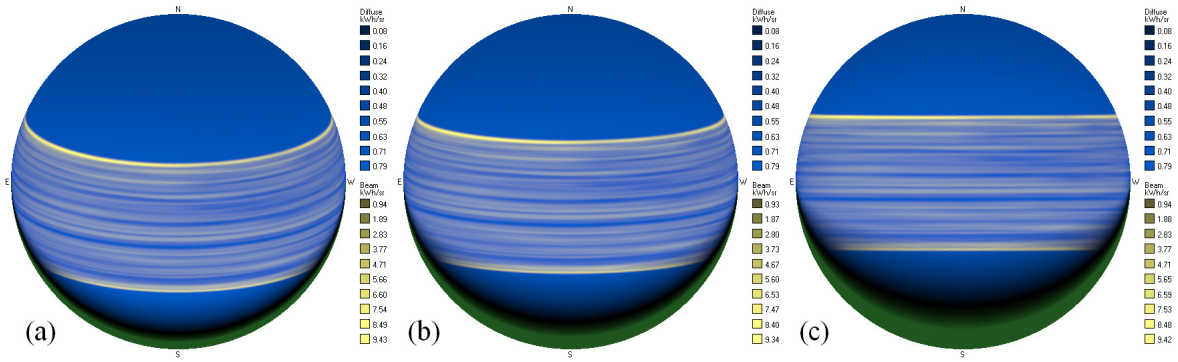

Fig. 7 Fisheye orthographic sky projections for Sofia, as seen from a row of PV panels: (a) on a 25°-tilted surface facing south; (b) on a 32°-tilted surface facing south; (c) on a latitude-tilt surface facing south for Sofia's latitude, 42.698°. The green and black colors represent the foreground and the sky shaded areas, respectively.

Using SOLARES to undertake all calculations for both the unobstructed and partially-obstructed sky cases, the results are illustrated in Fig. 8a for the latter case. With an angular resolution of 1°, the maximum beam tilted irradiation, H_b = 710.8 kWh/m^2, occurs at a tilt angle of 33° for both annual radiance databases. In the control experiment (with isotropic SVF), the maximum diffuse tilted irradiation (672.4 kWh/m^2) occurs for a tilt angle of 0° because the circumsolar radiance is ignored. This increases to 688.0 kWh/m^2 for a tilt angle of 13° with Igawa's model and 689.2 kWh/m^2 with the IGI model, again for a 13° tilt angle. The global tilted irradiance, $H_t = H_b + H_d$, reaches an annual maximum of 1318.2 kWh/m^2 for a tilt angle of 20° in the control experiment with isotropic SVF (Fig. 7a), 1373.7 kWh/m^2 for a tilt angle of 25° with Igawa's model, and 1374.8 kWh/m^2 for the same tilt angle of 25° with the IGI model. This angle is less than the local optimum angle under non-obstructed sky (32°, see Fig. 7b) or than the local latitude (42.698°, Fig. 7c). All results are summarized in Tables 2 and 3 for the unobstructed and partially obstructed sky cases, respectively.

Tab. 2: Maximum annual diffuse and global irradiation and optimum tilt for control experiment with SVF, Igawa's model and IGI model; unobstructed sky case

Irradiation	Control experiment (isotropic SVF)	Igawa's model	IGI model
Max. diffuse irradiation (kWh/m^2)	672.4 at tilt 0°	704.2 at tilt 22°	705.4 at tilt 22°
Max. global irradiation (kWh/m^2)	1347.3 at tilt 26°	1418.3 at tilt 32°	1419.5 at tilt 32°

Tab. 3: Maximum annual diffuse and global irradiation and optimum tilt for control experiment with SVF, Igawa's model and IGI model; partially obstructed sky case

Irradiation	Control experiment (isotropic SVF)	Igawa's model	IGI model
Max. diffuse irradiation (kWh/m²)	672.4 at tilt 0°	688.0 at tilt 13°	689.2 at tilt 13°
Max. global irradiation (kWh/m²)	1318.2 at tilt 20°	1373.7 at tilt 25°	1374.8 at tilt 25°

The difference in annual diffuse tilted irradiation between the two models (H_{dI} for Igawa's model, and H_{dCS} with CS improvement) varies almost linearly from 0.15% for a tilt of 0° to 0.24% for 90°. This translates into smaller differences (up to 0.1%) when rather considering the global tilted irradiance, as shown in Fig. 8a. It can be expected that significantly larger differences would be obtained in a sunnier climate.

In the literature, as used in many applications, SVF is estimated as the ratio between the non-obstructed part of the sky and the entire sky's circular projection. The underlying assumption is that the sky radiance is isotropic, which is only a crude approximation. A more accurate definition, referred to here as the Real Sky View Factor (RSVF), consists in taking the ratio between the radiation received by a planar surface under a partially obstructed sky of realistic (anisotropic) radiance and that received from the entire radiating sky hemisphere in the absence of shading.

The blue line in Fig. 8b represents RSVF as a function of tilt; the red line is the conventional SVF under the obstructions caused by the PV panel row to the south, denoted SVF_obstructed, and the green line is the SVF under an unobstructed sky. The difference between RSVF and SVF_obstructed varies from 0% for a horizontal surface to a maximum of 30% (relative to RSVF) for a tilt of 60°. These results confirm that the conventional SVF, based on the isotropic sky model, is a very imperfect tool. Even though this has been pointed out long ago (Johnson and Watson, 1984), the isotropic SVF paradigm is still used in the vast majority of applications.

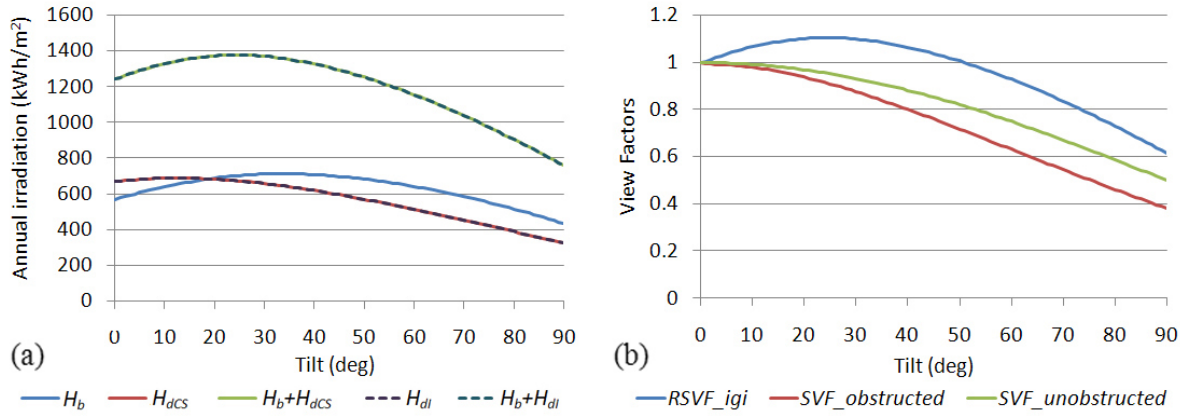

Fig. 8 Annual irradiation under partially obstructed sky for different tilt angles from 0° to 90° in Sofia: (a) Beam and diffuse irradiations and their sum; (b) Real SVF (with IGI model) and SVF for different tilts.

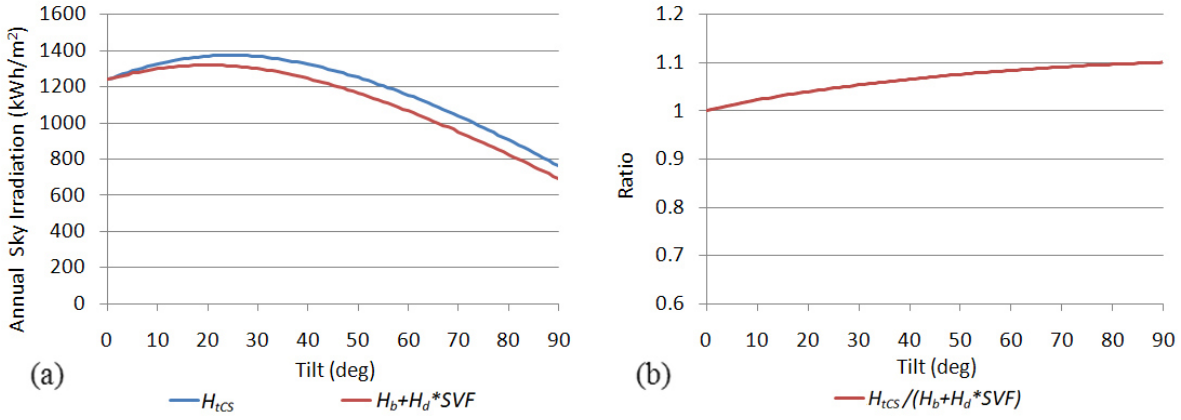

Fig. 9 Anisotropic vs. isotropic SVF approaches to estimate the tilted sky irradiation under a partially obstructed sky in 2014: (a) Annual sums of the total irradiation on various tilts; (b) Ratio between the anisotropic and isotropic results.

Figure 9 illustrates the results obtained with the approaches described above to estimate the sky diffuse tilted irradiation under a partially obstructed sky. The lower red line in Fig. 9a is for the control experiment, i.e., a naïve calculation based on the isotropic assumption, hence estimating the diffuse tilted irradiation as the product SVF•H_d. This conventional approach was followed by, e.g., Appelbaum (2018) to evaluate a catalog of SVFs applicable to various configurations of PV collector geometries. (Based on the results obtained here, this catalog would need to be revised to take anisotropic effects into account.) The blue line illustrates the more realistic result obtained with SOLARES and the IGI model. In particular, the annual optimal tilt is 25° for the anisotropic RSVF compared to 20° for the isotropic SVF.

Finally, Fig. 9b shows the relative improvement produced by the anisotropic radiance treatment (as calculated with the IGI model in SOLARES) in the partly obstructed sky case, compared to the control experiment. The IGI approach results in up to 10% higher global irradiance than the SVF approach, depending on tilt. Because the sky anisotropy is normally more pronounced under cloudless conditions, it can be expected that the difference just noted would increase when the diffuse ratio, K, decreases. For 2014 in Sofia, K is 0.54 on average, meaning that diffuse irradiation outweighs the direct beam component overall. It can be inferred that this difference would be significantly larger at sunnier sites, where the mean annual K can reach values lower than 0.25 (Gueymard, 2008b). Since sun elevation also plays a role, their interaction needs to be better understood.

6. Conclusion

Considering the paucity and current limitations of broadband measurements of the sky radiance or luminance with sky scanners, applications in engineering or architecture (among other fields) typically rely on simplified models. Despite being unrealistic, the isotropic model—simplest radiance distribution—is still commonly used in many applications, including the calculation of sky view factors (SVF) in the presence of sky shading.

In this contribution, the Igawa radiance/luminance model has been validated under the conditions of Colorado, whose low-turbidity climate at high elevation is in sharp contrast with that of the urban areas where this empirical model had been originally developed. Because of this model's lack of proper treatment of the circumsolar radiance within ≈6° from sun center, a specific circumsolar model has been proposed, using turbidity-dependent parameterizations based on SMARTS simulations. The combination of the original Igawa model and this circumsolar extension specific to the sun's aureole (if unobstructed by clouds) defines the newly proposed IGI model.

An application illustrating the improvement made possible by the consideration of anisotropic sky view factors in the case of either unobstructed or partly obstructed sky scenes has been demonstrated. It involves the calculation of annual tilted irradiations on tilted surfaces, using the SOLARES software (with the IGI model) and hourly irradiance time series from, e.g., TMY data. Significant differences are found between results obtained with the conventional approach (isotropic SVF) and its more realistic anisotropic replacement proposed here. This new IGI-based approach would be most beneficial at sunny sites. Further research is needed to (i) smooth the transition of radiance between the aureole and the rest of the sky hemisphere; (ii) better understand the intricate interactions between aerosol type, turbidity, cloudiness, and sun position; and (iii) validate the new radiance model with modern experimental equipment, such as high-resolution sky imagers.

References

Acosta, I., Munoz, C., Esquivias, P., Moreno, D., Navarro, J., 2015. Analysis of the accuracy of the sky component calculation in daylighting simulation programs. Sol. Energy 119, 54–67.

Appelbaum, J., 2018. The role of view factors in solar photovoltaic fields. Renew. Sust. Energ. Rev. 81, 161–171.

Blanc, P., Espinar, B., Geuder, N., Gueymard, C., Meyer, R., Pitz-Paal, R., Reinhardt, B., Renné, D., Sengupta, M., Wald, L., Wilbert, S., 2014. Direct normal irradiance related definitions and applications: The circumsolar issue. Sol. Energy 110, 561–577.

Brunger, A.P., Hooper, F.C., 1991. Measured shortwave radiance in an urban atmosphere. Sol. Energy 47, 137–142.

Brunger, A.P, Hooper F.C., 1993. Anisotropic sky radiance model based on narrow field of view measurements of shortwave radiance. Sol. Energy 51, 53–64.

Bullrich, K., 1964. Scattered radiation in the atmosphere and the natural aerosol. Adv. Geophys. 10, 99–200.

Burley, J.L., Fiorino, S.T., Elmore, B.J., Schmidt, J.E., 2017. A fast two-stream-like multiple-scattering method for atmospheric characterization and radiative transfer. J. Appl. Meteorol. Clim. 56, 3049–3063.

Chauvin, R., Nou, N., Thil, S., Grieu, S., 2015. Modelling the clear-sky intensity distribution using a sky imager. Sol. Energy 119, 1–17.

Darula, S., Kittler, R., Komar, L., 2015. Simulation of luminance sky patterns predetermining daylight illuminance on vertical house fronts with windows. Sol. Energy 120, 195–207.

Dubovik, O., King, M.D., 2000. A flexible inversion algorithm for retrieval of aerosol optical properties from Sun and sky radiance measurements. J. Geophys. Res. 105D, 20673–20696.

Gueymard, C.A., 1986. Une paramétrisation de la luminance énergétique du ciel clair en fonction de la turbidité. Atmosphere-Ocean 24, 1–15.

Gueymard, C.A., 2001. Parameterized transmittance model for direct beam and circumsolar spectral irradiance. Sol. Energy 71, 325–346.

Gueymard, C.A., 2008a. REST2: High-performance solar radiation model for cloudless-sky irradiance, illuminance, and photosynthetically active radiation – Validation with a benchmark dataset. Sol. Energy 82, 272–285.

Gueymard, C.A., 2008b. Fixed or tracking solar collectors? Helping the decision process with the Solar Resource Enhancement Factor. Proc. SPIE Conf. Vol. 7046, Optical Modeling and Measurements for Solar Energy Systems II, San Diego, CA.

Harrison, A.W., Coombes, C.A., 1988. Angular distribution of clear sky short wavelength radiance. Sol. Energy 40, 57–63.

Igawa, N., 2014. Improving the All Sky Model for the luminance and radiance distributions of the sky. Sol. Energy 105, 354–372.

Ivanova, S., 2015. Using of fisheye orthographic projection for cumulative estimation of direct and diffuse radiation on building surfaces in an urban environment. Proc. WREC XIV Conf., Bucharest, Romania.

Ivanova, S., Gueymard, C.A., 2018. Simulation and applications of cumulative anisotropic sky radiance patterns. Sol. Energy (in review).

Johnson, G.T., Watson, I.D., 1984. The determination of view-factors in urban canyons. J. Appl. Meteorol. Clim. 23, 329–335.

Kittler, R., 1994. Some qualities of scattering functions defining sky radiance distributions. Sol. Energy 53, 511–516.

Kocifaj, M., 2009. Sky luminance/radiance model with multiple scattering effect. Sol. Energy 83, 1914–1922.

Kocifaj, M., 2011. CIE standard sky model with reduced number of scaling parameters. Sol. Energy 85, 553–559.

Kocifaj, M., 2012. Angular distribution of scattered radiation under broken cloud arrays: An approximation of successive orders of scattering. Sol. Energy 86, 3575–3586.

Kocifaj, M., 2015. Unified model of radiance patterns under arbitrary sky conditions. Sol. Energy 115, 40–51.

Kocifaj, M., Gueymard, C.A., 2017. High-resolution tilted surface illuminance/irradiance spectral model applicable to arbitrary sky conditions. Proc. Lux Europa Conf., Ljubljana, Slovenia.

Li, D.H.W., Lam, T.N.T., 2007. Determining the optimum tilt angle and orientation for solar energy collection based on measured solar radiance data. Int. J. Photoenergy 2007, 85402.

Liang, S., Lewis, P., 1996. A parametric radiative transfer model for sky radiance distribution. J. Quant. Spec-

trosc. Radiat. Transfer 55, 181–189.

Lou, S., Li, D.H.W., Lam, J.C., Lee, E.W.M., 2016. Estimation of obstructed vertical solar irradiation under the 15 CIE Standard Skies. Build. Environ. 103, 123–133.

Nakajima, T., Tonna, G., Rao, R., Boi, P., Kaufman, Y., Holben, B., 1996. Use of sky brightness measurements from ground for remote sensing of particulate polydispersions. Appl. Opt. 35, 2672–2686.

Oliveros, C.S., Reyes, F.J.O., Alados-Arboledas, L., 1998. Determination of aerosol optical thickness from measurements of spectral sky radiance. J. Aerosol. Sci. 29, 1199–1211.

Perez, R., Seals, R., Michalsky, J., Steward, R., 1993. All-weather model for sky luminance distribution—preliminary configuration and validation. Sol. Energy 50, 235–245.

Qin, Y., Box, M.A., Jupp, D.L.B., 2002. Inversion of multiangle sky radiance measurements for the retrieval of atmospheric optical properties—1. Algorithm. J. Geophys. Res. 107D, doi:10.1029/2001JD00094.

Rosen, M.A., Hooper, F.C., Brunger, A.P., 1989. The characterization and modelling of the diffuse radiance distribution under partly cloudy skies. Sol. Energy 43, 281–290.

Smith, C.J., Forster, P.M., Crook, R., 2016. An all-sky radiative transfer method to predict optimal tilt and azimuth angle of a solar collector. Sol. Energy 123, 88–101.

Torres, J.L., Torres, L.M., 2008. Angular distribution of sky diffuse radiance and luminance. In: Badescu, V. (Ed.), Modeling Solar Radiation at the Earth Surface. Springer, pp. 427–448.

Tregenza, P.R., 1987. Subdivision of the sky hemisphere for luminance measurements. Light. Res. Technol. 19, 13–14.

Vida, J., Foyo-Moreno, I., Alados-Arboledas, L., 1999. Performance validation of MURAC, a cloudless sky radiance model proposal. Energy 25, 705–721.

Wittkopf, S.K., Soon, L.K., 2007. Analysing sky luminance scans and predicting frequent sky patterns in Singapore. Lighting Res. Technol. 39, 31–51.

Zibordi, G., Voss, K.J., 1989. Geometrical and spectral distribution of sky radiance: comparison between simulations and field measurements. Remote Sens. Environ. 27, 343–358.

Appendix

Coefficients A_i in Eq. (1) are provided by the equations below, valid for β strictly >0.

$$A_0 = \{b_2/(b_0\beta)\} \exp\{-0.5[(\ln\beta - b_1)/b_0]^2\}$$

$$A_1 = (c_0 + c_1\beta)/(1 + c_2\beta + c_3\beta^2)$$

$$A_2 = (d_0 + d_1\beta)/(1 + d_2\beta)$$

where

$$b_0 = (2.4413 + 0.77346m + 0.0066318m^2)/(1 + 0.71507m)$$

$$b_1 = (5.4847 - 1.7750m - 0.028094m^2)/(1 + 0.94430m)$$

$$b_2 = (98.386 + 21.399m - 0.48309m^2)/(1 + 3.6764m)$$

$$c_0 = m\,(0.50144 + 0.071324m)/(1 + 0.15932m + 0.059551m^2)$$

$$c_1 = m\,(4.4497 - 29.822m)/(1 + 1.1167m + 0.046374m^2)$$

$$c_2 = m\,(77.474 - 4.2505m)/(1 + 1.9922m + 0.19715m^2)$$

$$c_3 = (2171.9 - 2352.3m + 1696.0m^2)/(1 + 41.4m - 0.99879m^2)$$

$$d_0 = (2.1308 + 17.274m + 1.2349m^2 + 0.017568m^3)/(1 + 9.0143m + 1.3056m^2)$$

$$d_1 = (-0.28158 + 0.18907m - 0.067057m^2 + 0.0030898m^3)/(1 - 0.17939m + 0.03345m^2)$$

$$d_2 = (-0.14376 + 0.43815m - 0.10685m^2 + 0.0094731m^3)/(1 - 0.1235m + 0.025835m^2)$$